Factors Leading to the Formation of a Resistive Thin Film at the Bottom of Aluminum Electrolysis Cells

MARC-ANDRÉ COULOMBE, GERVAIS SOUCY, LOIG RIVOALAND, and LYNNE DAVIES

Studies on sludge formation in aluminum electrolysis cells are rare and typically do not distinguish the deposits at the center of the cell from those composing the ledge toe because low voltage lost is expected at the center of the cell. However, high amount of sludge in the center leads to the formation of a thin film in an intermediate zone between the ledge toe and this center thick sludge accumulation. Looking at sludge deposits through composition mapping and microstructure analysis coming from four aluminum cells of two different aluminum reduction technologies, major factors leading to a thin resistive film were identified. This includes the formation of a suspension on the top of the thick deposit at the center of the cell, its displacement through magnetohydrodynamic induced movement by the metal pad, and the growth and thickening of a carbide sublayer making the thin film even more resistive. Correlation between thickening of the thin film and cathode voltage drop increase was observed. The postmortem analysis performed on six laboratory experiments was found useful to support different observations made on the industrial cells at lower cost.

I. INTRODUCTION

HALL–HEROULT cells from the aluminum electrolysis industry often encounter incomplete dissolution of alumina through many types of events enabling the agglomerations to sink and form sludge.[1] This phenomenon will depend heavily on the alumina physical properties.[2] Secondary feeding from the anode cover material, a mixture of crushed bath and alumina protecting the anode, and backfeeding of the sludge itself add uncertainty to the alumina concentration in the bath.[3] Moreover, changes in the heat losses at the cell wall may influence the amount of sludge generated from the side towards the center of the cell.[4] The presence of this sludge can lead to the formation of resistive deposits, an increase in the length of the current path, the deterioration of the cathode block, and even the premature stoppage of the cell.[5] Figure 1 presents the different zones found in the Hall–Heroult cell.

The study of deposits formation at the center of the cell is necessary to extend the general understanding of the path that the smelter grade alumina (SGA) follows from the top of the bath to the bottom of the cell. It is known that SGA, while in bath, will undergo a γ-Al_2O_3 to α-Al_2O_3 phase transformation and agglomeration that can lead to incomplete dissolution.[6] Electrolytic bath will infiltrate the agglomerate and may cause the SGA to transport some bath material under the metal pad if its weight overcomes the surface tension between the bath and the metal.[7] Previous work on CFD modeling showed that alumina could be mixed in the bath through gas release beneath the anode, the interaction of the magnetic and electric fields in the bath, the drag in the metal from MHD-induced movement and thermal convection.[8] The previous study also showed that mixing via center and end channels was a faster process than alumina consumption. It could then be concluded that while SGA concentrated in the bath under the SGA feeders, this same SGA will also tend to spread along the central channel.

Extended works performed by Geay et al. on metal/bath liquid height differential along cathode blocks demonstrated that most of the material that sinks under the metal pad will preferentially deposit in the central channel.[1] The study suggested three reasons why sludge accumulations were higher in the central channel:

– SGA feeding takes place along the central channel and when alumina does not dissolve properly, it produces sludge in that area.
– The crust is fragile in that area and can form sludge after its collapse.
– During covering practices, significant quantities of the covering material are added in the central channel, contributing to an increased production of sludge in that area.

MARC-ANDRÉ COULOMBE, Graduate Student, and GERVAIS SOUCY, Professor, are with the Department of Chemical and Biotechnological Engineering, Université de Sherbrooke, 2500 Boulevard de l Université, Sherbrooke, QC, J1K 2R1, Canada. Contact e-mail: Gervais.Soucy@USherbrooke.ca LOIG RIVOALAND and LYNNE DAVIES, Researchers, are with Rio Tinto (Arvida Research and Development Centre), 1955 Boulevard Mellon, Jonquière QC, G7S 4K8 Canada.
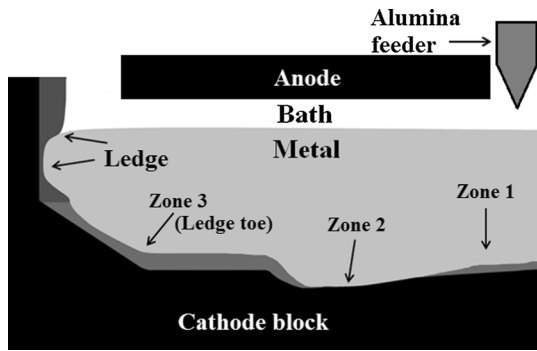
Fig. 1—Schematic of the Hall–Heroult cell with the different zones.

Another work on sediment transport and dissolution in Hall–Heroult cell, performed by Tørklep *et al.*, concluded that turbulent movements in the metal can disperse some free flowing Al_2O_3 particles[9] and that the sludge dispersion following SGA feeding could happen before and after settling. This study put forward that larger lumps coming from the anode cover will most likely settle on the cathode block surface under the central channel. Hence, any hardened sludge will not disperse much.

Another study performed by Thonstad *et al.* showed that sufficient heat dissipation through the bottom of the cell will harden the sludge through the formation of α-Al_2O_3 hexagonal platelets.[10] Deposits found on the cathode block surface will contain, depending on the position of the cell, Al_2O_3 particles in a liquid electrolytic bath (bottom sludge), solid Al_2O_3 particles frozen in a solid–liquid bath (bottom crust), or a cryolite supersaturated solid–liquid bath (bottom freeze).[4] A completely liquid bath can also be found under the metal pad and is defined as 'bath film.' When the film was not completely liquid and was composed of an Al_2O_3 supersaturated bath, it was referred as 'thin film.'

Previous studies have discussed the different characteristics of the ledge toe. In this paper, we expand the analysis to the deposit formation at the center of the cell and show that these deposits can participate in the deterioration of the cathode block by the formation of secondary resistive thin film between the central channel and the ledge toe.

II. ELECTROLYSIS CONDITIONS AND PARAMETERS

Aluminum electrolysis experiments were performed at laboratory scale in order to study the deposit formation occurring under the metal pad of Hall–Heroult cells. Each experiment had a side with a cooled wall and a SGA feeding side. The electric current was directed towards the cooled side where the ledge toe was expected, by connecting the cathode bar only on this side. This produced a high current density zone on the cooled side similar to what can be expected in industrial cell. Pure aluminum plates were added to the electrolysis cell at the beginning of the experiment before adding

solid bath in order to create a chemical barrier between the electrolytic bath and the formed deposits at high temperature. This setup was performed to simulate the thermal, mass, and electrical gradients that exist in real industrial cells during operation. An unavoidable scale effect from this setup was that the MHD-induced movements and thus the back-feeding rate in the laboratory cell differs significantly from what can be found in industrial cells. Figure 2 shows the front view of the laboratory electrolysis cell.

Cathode block was 130 mm (W) × 175 mm (L) × 200 mm (H) in which a pocket of 80 mm (W) × 120 mm (L) × 150 mm (H) was machined to contain the bath and the metal. The initial amounts of industrial bath and pure aluminum added were 1600 and 550 g, respectively. The bath had a molar ratio (NaF/AlF_3), called cryolite ratio (CR) of 2.20 and contained a mass composition of 5 pct CaF_2 and 10 pct Al_2O_3. The industrial cells are autothermic, while the small-scale laboratory cells need external heat and are thus typically isotherm. The electrolysis was then carried out at 1228 K (955 °C) using a nitrogen gas cooler to drop the temperature of one side of the carbon cathode to simulate the frozen side of an industrial cell wall. The electrolysis cell was placed in an Inconel crucible inside a circular furnace. The cooled wall temperature was measured using the thermocouple T_1. The furnace temperature was controlled through the thermocouple T_2 located in the wall of the cathode block near the SGA feeding point. The cooled wall was always insulated from the external furnace on the side in order to create a temperature gradient in the cell. Additional insulation was added for specific experiments to isolate the gas cooler from air convection and radiation to further increase the heat transfer while maintaining the same nitrogen flow rate of 13 L/min (see Figure 3). In anticipation of studying the cathode voltage drop (CVD), experimental tests had three or four alumina plates to constrain the cathode surface area. The ledge toe formation occurred only if the fourth plate was absent, but it was not possible to certified that the ledge toe effectively constrained the cathode surface area The total current was set at 70 A. This gave a current density of 0.9 A/cm² at the cathode block surface when four alumina plates were used. The anode-cathode distance was maintained at 2 cm. Figure 3 shows a top view of the experimental cell:

SGA was fed by pulses of approximately 10 to 20 seconds, every 3 minutes using a K-Tron powder feeder. The SGA feeder was located on the side opposite to the cooling to simulate the point feeder in the central channel of industrial cells. Each experimental test began with 2 hours of electrolysis without SGA feeding. This first step was completed to build the ledge toe and to stabilize the temperature of the cell. The second step of electrolysis took 5 hours and the feeding rate for this step was set to 120 pct of the theoretical consumption value for tests A to E and 150 pct for Test F. The second step lasted only 3.5 hours for Test F due to uncontrolled voltage rise. The important conclusions of this test are discussed later in this paper. The efficiency was calculated from the aluminum production of the preliminary

experiments derived from the theoretical production calculated with Faraday's laws. The feeding rate was based on 60 pct current efficiency confirmed on previous laboratory tests without SGA feeding. The current was not confirmed in this series of experiments with SGA feeding as aluminum metal was mixed with sludge and resulted in mass measurement uncertainty.

The electrolysis test A was compared to Test B to evaluate the impact of the type of cathode material on the deposits formation. Graphitized material was made of petroleum coke and coal tar pitch heat treated at 3273 K (3000 °C), while 100 pct graphitic material was made of graphite and coal tar pitch baked at 1273 K (1000 °C). The thermal conductivities at operation temperature 1233 K (960 °C) for such material are 67.5 and 27.0 W/m K, respectively.[11] Test A was compared to Test C to evaluate the effect of the heat transfer rate that was measured by the cooled wall temperature. The tests C and D for the graphitized material and the tests B and E for graphitized material were performed to evaluate the insulating effect of an alumina plate on the cooled side on the deposit formation. Table I compares the electrolysis parameters of each test.

A. Sample Preparation

Nitrogen air flow was kept at 2.5 L/min during cooling after electrolysis to avoid an oxidation of the graphite lining in the Inconel crucible until the thermocouple located in the wall of the cathode block indicated 373 K (100 °C). The cathode block was then transferred into an argon-filled glove box where it cooled down to room temperature. Samples were collected three days after the cells were stopped. The composition and morphology of laboratory samples were compared with industrial samples using a similar postmortem analysis procedure as shown in Figure 4.

To extract samples from the laboratory postmortem cells, a first cut was done 15 mm over the cathode surface. The bottom part was then cut into two parts to study (1) the morphology with a scanning electron microscope and (2) the chemical composition of the deposits by Rietveld analysis (see Figure 4).

B. Characterization

The deposit samples were crushed, placed in a rotating sample holder ($1 s^{-1}$), and analyzed by a PANalytical X'Pert PRO MPD diffractometer using a Cu Kα X-ray tube under a Bragg-Brentano configuration. The X-Ray was filtered through a nickel film (0.0200 mm), and the XRD pattern was acquired with a PIXcel[1D] detector. The measurement was collected from 10 to 74 deg 2θ angle, with a spatial resolution of 0.0263 deg, and a time step of 0.12 seconds. The calcium content was measured with a XRF Potflux Channel.

Samples of the interface between the cathode block and the deposit were carefully prepared in thin slices (see Figure 4) and observed in a Hitachi S-4700 scanning electron microscope. The acceleration voltage was set at 20 kV, the intensity of the beam at 10 μA, and the working distance at 12 mm. Elemental analysis was performed using an Oxford X-Max 50 mm² Energy-dispersive X-ray spectroscopy module (EDS).

The solid–liquid equilibrium was calculated at 1233 K (960 °C) for α-Al_2O_3 and Na_3AlF_6 using the FactSage 6.4 software. This software relies on the Gibbs free energy minimization to produce phase diagram for the chemical composition provided by the Rietveld analysis of the samples.
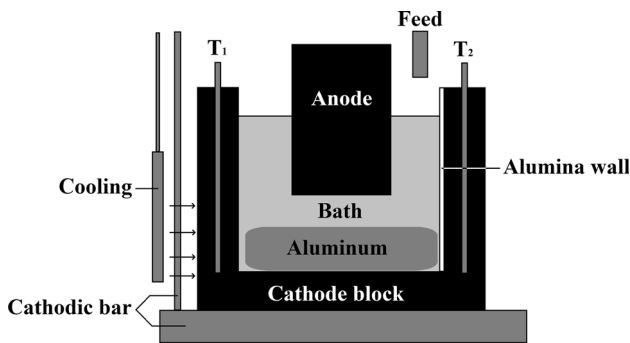

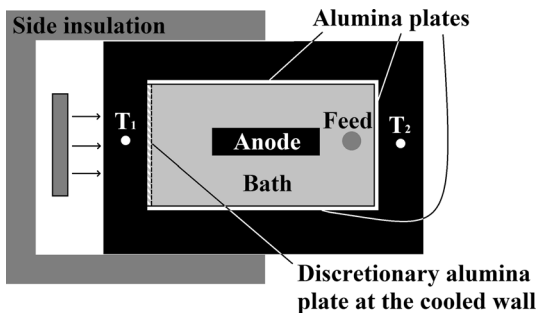Fig. 2—Front view of the electrolysis cell.

Fig. 3—Top view of the electrolysis cell.

Table I. Experimental Electrolysis Parameters

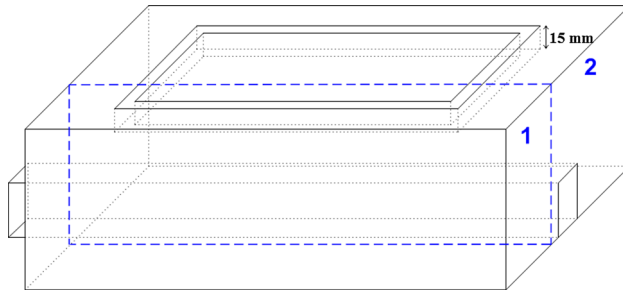| Test	Cathode Material	Heat Transfer Rate	Alumina Plate at the Cooled Wall	SGA Feeding Rate (Pct)	Electrolysis Time (h)
A	graphitized	high	no	0 to 120	2 to 5
B	100 pct graphitic	high	no	0 to 120	2 to 5
C	graphitized	low	no	0 to 120	2 to 5
D	graphitized	low	yes	0 to 120	2 to 5
E	100 pct graphitic	high	yes	0 to 120	2 to 5
F	graphitized	low	no	0 to 150	2 to 3.5

Fig. 4—Lower part of cathode with (*1*) smaller part for the study of the deposit morphology and (*2*) larger part for chemical composition analysis.

The density gradient between the deposit and the metal pad has been estimated by subtracting the aluminum density at 1233 K (960 °C) to the weighted average of the density of the liquid fraction and the solid fraction of the deposit. The density of the liquid fraction of the deposit was calculated according the relation synthesized by Solheim[12]:

$$\rho_T (\text{kg/m}^3) = \rho_{1273\,\text{K}\,(1000\,°C)} - b(T - 1000), \quad [1]$$

where ρ_T is the liquid fraction density at a given temperature, $\rho_{1273\,\text{K}\,(1000\,°C)}$ is the liquid fraction density at 1273 K (1000 °C), T is the temperature in °C, and Parameter b is a temperature correction factor, which is defined as follows:

$$b = 0.64 x_{\text{NaF}} + 0.39 x_{\text{CaF}_2} - 1.8 x_{\text{Al}_2\text{O}_3} + \frac{1.7 x_{\text{CaF}_2} + 1.5 x_{\text{AlF}_3}^2}{1 + 140 x_{\text{NaF}} x_{\text{AlF}_3}^5}, \quad [2]$$

where x is the mass fraction of NaF, AlF$_3$, CaF$_2$, and Al$_2$O$_3$ accordingly.

The density of the electrolytic bath is calculated at 1273 K (1000 °C) as a function of the corrected concentrations with the equation:

$$\rho_{1273\,\text{K}\,(1000\,°C)} = \left[(1946 + 1113 x_{\text{AlF}_3})^{-3.6} + \left(\frac{x_{\text{AlF}_3}}{859} \right)^{3.6} \right]^{-1/3.6}$$
$$+ \frac{780 x_{\text{CaF}_2}}{1 + 0.06 x_{\text{CaF}_2}} - \frac{9000 x_{\text{Al}_2\text{O}_3} x_{\text{AlF}_3}}{1 + 12 x_{\text{Al}_2\text{O}_3}} \quad [3]$$

The solid fraction in the deposit can be either α-Al$_2$O$_3$ or Na$_3$AlF$_6$. The calculated density of α-Al$_2$O$_3$ at 1233 K (960 °C) is 3890 kg/m^3,[13] about 2500 kg/m^3 for solid Na$_3$AlF$_6$,[14] and 2300 kg/m^3 for liquid aluminum.

III. RESULTS

A. Sample Mapping in the Industrial Cell

The chemical composition and morphological properties of industrial samples were obtained from four cells using two different technologies. The cells were stopped by removing the current connectors. Most of the bath and aluminum was extracted. The cells cooled down with a small amount of remaining aluminum that was extracted after it was solidified. Powder material was vacuumed without scratching the bottom to observe the deposits attached to the carbon block. Samples were collected approximately one week after the cells were stopped, allowing the cells to cool down to a safe working temperature. Table II compares the characteristics of each industrial cell.

The observations of the Technology I cathode surface block during postmortem analyses showed three distinct deposit zones (1) a whitish deposit found under the SGA feeder, (2) an intermediate yellowish-grayish film zone, and (3) a grayish deposit on the side known as ledge toe (see Figure 1). The zone 1 deposit was different in aspect for Technology II cathode surface block, while zones 2 and 3 were similar in aspect. The zone 1 in Technology II deposit depicted a dark deposit covered with a whitish deposit found in the central channel. The dark deposit was composed of an Al$_4$C$_3$ layer covered with thick deposits that were detached at some places by the aluminum pad removal after cooling. While previous studies focused on the ledge toe,[4,15] this study analyses more deeply the Zone 1 and Zone 2 deposits.

The cells a and b from Technology I were made of graphitic cathode blocks and possessed two SGA point feeders and two anode risers. They operated from 0.82 to 0.97 A/cm^2 according to the theoretical surface with rising amperage, with a metal pad height between 12 and 14 cm, and were stopped after 1413 and 1667 days of operation, respectively. The cells a and b were targeted according to their CVD. On average, Cell a had a higher voltage drop and also more deposits than Cell b. The shape of the deposits found under the SGA feeder and the length of the ledge toe, typical of Technology I cells, are shown in Figure 5.

The velocity profile in the metal for Technology I contained two main MHD-induced rotating patterns at each end of the cell and four secondary rotating patterns in between. The left circular swirl and the two right secondary swirls turn clockwise. The right swirl and the two left secondary swirls turn counter clockwise. The bottom part of the left swirl, the right swirl, and the top left secondary swirl fit well with the ledge toe profile. However, nothing in the simulation of the velocity profile explained the presence of the deposits under the SGA feeders.

The cells c and d from Technology II were made of graphitized cathode blocks, and possessed four SGA point feeders and five anode risers. The central channel was larger than in the cells of Technology I. The cells c and d were operated from 0.81 to 0.95 A/cm^2 also according to the theoretical surface with rising amperage, with the same metal level as Technology I and were stopped after 1204 and 2593 days, respectively. The cells c and d were also targeted according to their CVD. On average, Cell d had a higher voltage drop and also more deposits than Cell c. The shape of the deposits at the central channel and the length of the ledge toe, typical of Technology II cells, are shown in Figure 6.

The velocity profile in the metal for Technology II contained two main MHD-induced rotating patterns, the left one taking 2/3 of the cell and the right one 1/3. The left circular swirl turns counter clockwise and fits

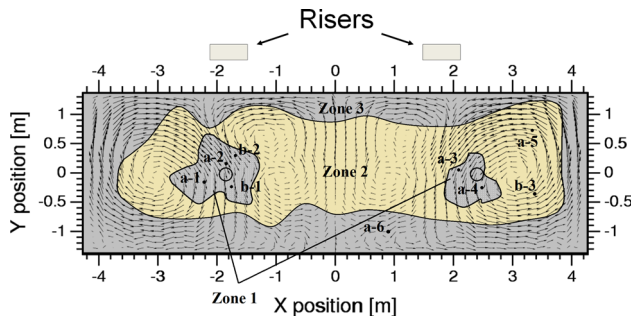| Cell	Technology	Cathode Block	Age (Days)	CVD
a	I	graphitic	1 413	typically high
b	I	graphitic	1 667	typically low
c	II	graphitized	1 204	typically low
d	II	graphitized	2 593	typically high

Fig. 5—Schematic view of the measured deposit formation and sampling position (*a-1* to *a-6* and *b-1* to *b-3*) along with the velocity profile based on the work of Renaudier *et al.*[21] in the metal for a typical cell of Technology I. The modeled velocity profile is calculated without deposit. Circular shapes—feeding point. Gray Zone 1—whitish deposits under the SGA feeder. Yellow Zone 2—thin film. Gray Zone 3—ledge toe.
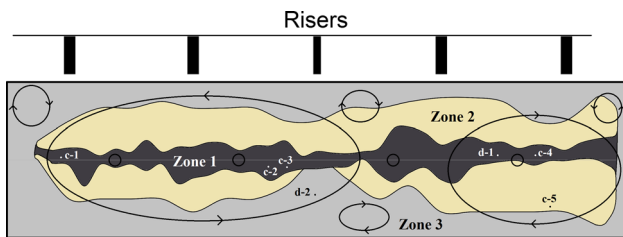

Fig. 6—Schematic view of the measured deposit formation and sampling position (*c-1* to *c-5* and *d-1* to *d-2*) for a typical cell of Technology II. Small circular shapes—feeding point. Larger circular shapes—velocity profile based on the work of Renaudier *et al.*[21] The modeled velocity profile is calculated without deposit. Dark Zone 1—thick deposits along the central channel. Yellow Zone 2—thin film. Gray Zone 3—ledge toe.

well with the ledge toe profile. The right swirl turn clockwise and a small counter clockwise eddy on the right top corner explain the ledge toe profile. However, nothing in the simulation of the velocity profile explained the presence of the deposits in the central channel.

B. Deposits in Zone 1 at the Center of the Industrial Cells

Deposits at the center of cells *a* and *b* were whitish rounded spots found under the SGA feeder and were 0.5 to 9 mm. The deposits of cells c and d did not particularly accumulate under the SGA feeders, and were visually different for the deposits of the cells a and b. They were mostly aluminum carbide dark stripes covered with a whitish deposit 3- to 50-mm thick in the central channel. During the postmortem analysis, the floor contained relatively few remaining thick deposits.

The dark and almost carbon black aspect of the stripe gave the impression that the cathode blocks were uncovered. However, systematic removal of the residual thick deposits revealed the dark surface. For both technologies, the cell that had the most deposit in Zone 1 during the postmortem analysis was associated with the highest CVD just before its shut down.

The whitish deposits found under the SGA feeder of Cell a covered 3 and 9 pct of the total cathode surface. In order to study the formation of the deposits found under the SGA feeder, four samples were extracted (a-1 to a-4). SEM-EDX analysis of sample a-4 showed that cryolite deposits of 0.5 to 4 mm covered the cathode block under the SGA feeder. A thin aluminum carbide sublayer of 25 to 75 μm was also present at the interface between the deposit and the carbon cathode block.

Cell *b* generally had small amounts of whitish deposits that were generally less charged in solid alumina. The whole cell b contained less deposit overall. The deposit areas under the SGA feeder took 1 and 3 pct of the total cathode surface and the ledge toe was 2 pct shorter on the downstream and 40 pct shorter on the upstream than Cell a ledge toe. Two samples were cored on the larger deposit (b-1 and b-2). Deposit thicknesses were between 1 and 9 mm for the b-1 sample and 5 to 8 mm for the b-2 sample. A similar aluminum carbide thin layer found under deposits of Cell a had a thickness of 30 to 100 μm for the b-1 sample and 10 to 75 μm for the b-2 sample. Hexagonal alumina platelets were found for both cells a and b with diameters ranging from 50 to 700 μm.

The thick whitish deposit in the central channel of Cell c covered in average 16 pct of the total cathode surface and had a minimum block coverage of 5 pct and maximum block coverage of 35 pct. SEM-EDX and XRD analysis of a plane surface showed that a thin layer of 400 to 700 μm (Figure 7), composed of Al_4C_3 (63 pct), Na_3AlF_6 (6 pct) of $Na_5Al_3F_{14}$ (9 pct), Al_2O_3 (13 pct) and carbon (6 pct), was present. The composition gave a low CR (1.97). The SEM-EDX analysis also showed the presence of α-Al_2O_3 hexagonal particles of 30 μm in diameter and 4-μm thick in the thin layer. Among the thick deposit still present in the central channel, four samples were taken (c-1 to c-4). The deposits thickness varied between 3 and 50 mm. MEB-EDX analysis showed alumina particle size between 5 and 30 μm in the bulk of the whitish deposit and 10 to 80 μm on the top.

The deposits in the central channel of Cell *d* were almost completely absent during postmortem analysis. Visual observations indicated that the thick deposits covered in average 17 pct of the total cathode surface

and had a minimum block coverage of 0 pct and maximum block coverage of 37 pct during operation. The block uncovered with the thick deposit was positioned in a high-speed zone in the middle of the main rotating pattern. The presence of thick deposits embedded in the cooled metal pad was observed for Cell d but no sample could be extracted for logistical reasons. However, enough material remained on the cathode block to extract one sample (d–1) that supported a higher alumina concentration in Technology II central channel deposits.

The chemical composition and thermodynamic properties of the deposits found in Zone 1 at the center of the industrial cells are shown in Table II. The amorphous content of the sample is given to quantify the uncertainty of the deposit composition that could not be measured by XRD. To reduce this uncertainty, the total Al_2O_3 content was estimated by elemental oxygen analysis and the total Ca content was measured by XRF. Deposit samples at operation temperature are often composed of a bath liquid fraction and solid alumina. The total mass concentration gradient of AlF_3 and CaF_2 can be fixed between two deposit samples in the bath liquid fraction while significantly varying in the total concentration due to a diluting effect of the presence of solid alumina.[15] To improve the understanding of deposit behavior, CR and CaF_{2eq}, independent of the alumina content, were calculated. The temperature of crystallization and the amount of $Na_3AlF_{6(s)}$ and $Al_2O_{3(s)}$ at 1233 K (960 °C) have been predicted using FactSage software based on the composition of the samples measured by XRD. The density gradient between the deposit and the metal pad has been estimated. Vertical composition gradient was studied by cutting several slices. The bottom slice close to the carbon cathode block is named S1 and top slice S2, S3, and S4. Table III presents the summary of all sample chemical composition found in Zone 1 industrial cells.

The CR of the deposits sampled in Zone 1 for both technologies (2.24 to 2.63) is usually higher than the electrolytic bath (2.20). There are indications that the composition of the deposit is lower in $CaF_{2(eq)}$ for Technology I. The tendency to have low solid Al_2O_3 concentrations for Technology I samples is even stronger and this low concentration has a direct impact on the temperature of crystallization and the density gradient of the deposits. For Technology I thinner samples, their density can be lower than liquid aluminum. For Technology II thicker samples, the density can be much higher than the metal pad density. The temperature of crystallization of Na_3AlF_6 is predominantly influenced by the concentration of AlF_3 and the CaF_2. As their mass concentration increases, the temperature of crystallization of Na_3AlF_6 decreases.

In terms of vertical gradient, the Al_2O_3 mass concentration and the associated density presented the most important variation. As an example, the top layer density of sample c-3-S4 is lower than the density of the rest of the sample and approaches the aluminum metal pad density.

C. Thin Film in Zone 2 (Industrial Cells Intermediate Zone)

Questions about the presence of a bath film between the ledge toe and the metal pad have interested the aluminum industry. In this paper, this area is called the intermediate zone or Zone 2. It was not always possible to study the chemical composition of such a film everywhere in the intermediate zone due to film thickness. However, the thin film was still studied by SEM-EDX when it was too thin. Analysis confirmed that the thin film was present everywhere between the cathode block and the metal pad.

For both technologies, the thin film covered the remaining cathode surface not covered either by the deposit at the center of the cell or by the ledge toe. The color of the thin film in the intermediate zone ranged from yellowish to grayish. The larger the area of the surface that was covered by the Zone 1 deposit and ledge toe, the more the thin film looked grayish. For both technologies, cells with a more grayish film in the intermediate zone were associated with a higher CVD just before shut down. Specific data on the thin film were studied by extracting a chunk of the cathode block in each cell.

A typical sample of the thin film (a-5) was collected in Cell a in order to study the local covering of the cathode block and several measurements were made. The film covered 20 pct to 40 pct of the sample surface and had a thickness from 0.2 mm to 5 mm. The remaining was made of the very thin yellowish film. The procedure was repeated for Cell b by extracting a chunk of the cathode block (b-3) that was similar to Cell a sample (a-5) local aspect. It was concluded that for similar aspect of the cathode block, the local covering tended to be similar. However, observation of the Cell b thin film in the intermediate zone during postmortem analysis tended to be generally more yellowish than Cell a and its CVD lower during its cell life in general. Further investigation could not be performed due to rapid degradation of the Al_4C_3 thin layer.

A typically very yellowish film and a typically very grayish (c-5) film were collected in Cell c (Figure 8). The morphology of the two types of film was investigated by SEM-EDX but only c-5 sample could generate enough material to be investigated by XRD analysis.

The yellowish film (Figure 8(a)) was made of a heterogeneous Al_4C_3 layer ranging from 0 to 15 μm and a very thin layer ($<$1 μm) of bath component at the surface. Some hexagonal alumina particles could be observed. The particles observed were between 20 μm and 35 μm of diameter and had a thickness of 2 μm. The straight cut in the thin film (Figure 8(b)) showed that the residual deposit layer somehow delaminated from the cathode block. The total thickness of the deposit was about 0.5 to 1.5 mm. The grayish film enabled the growth of the Al_4C_3 sublayer and homogenized its thickness ranging from 10 to 20 μm. The study of the morphology of the Al_2O_3 hexagonal platelets shows that the diameter of the particles ranged from 50 to 150 μm.

The intermediate zone in Cell d contained a region with thick whitish deposits that had not been observed

C Ka1_2 F Ka1_2 Al Ka1
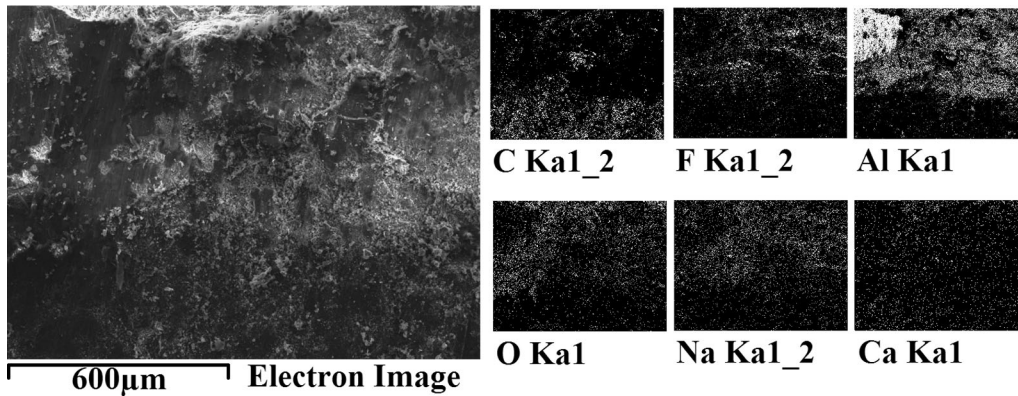
O Ka1 Na Ka1_2 Ca Ka1

600μm Electron Image

Fig. 7—MEB-EDX analysis of the dark thin layer under the thick sludge deposit at the center of the cell.

Table III. Chemical Composition of Deposit Found in Zone 1 at the Center of Industrial Cells

Sample	Na_3AlF_6 (Pct)	CaF_2 (Pct)	AlF_3 (Pct)	Al_2O_3 (Pct)	Amorph. (Pct)	CR	$CaF_{2(eq)}$ (Pct)	$T_{crist.}$ Na_3AlF_6 K (°C)	$T_{crist.}$ Al_2O_3 K (°C)	$Al_2O_{3(s)}$ 1233 K (960 °C) (Pct)	$Na_3AlF_{6(s)}$ 1233 K (960 °C) (Pct)	$\Delta\rho$ 1233 K (960 °C) kg/m^3
a-1	56.2	4.7	6.2	33.0	13	2.35	6.4	1210 (937)	1817 (1544)	27.5	—	278
a-2	67.8	5.5	5.4	21.7	—	2.50	6.4	1215 (942)	1565 (1292)	15.2	—	40
a-3	56.8	4.6	5.4	33.3	17	2.42	6.4	1213 (940)	1819 (1546)	27.8	—	277
a-4	74.0	5.3	4.9	15.9	21	2.58	5.8	1218 (945)	1411 (1138)	8.7	—	(89)
b-1-S1	78.7	5.9	4.4	11.0	—	2.63	6.1	1218 (945)	1303 (1030)	3.5	—	(189)
b-1-S2	79.1	5.3	5.8	9.8	29	2.54	5.5	1218 (945)	1274 (1001)	2.1	—	(211)
b-2-S1	77.0	5.3	4.5	13.3	23	2.62	5.6	1219 (946)	1349 (1076)	5.9	—	(148)
b-2-S2	79.9	5.4	5.4	9.3	12	2.57	5.5	1218 (945)	1263 (990)	1.5	—	(223)
c-1	40.9	4.1	4.8	50.2	10	2.32	7.7	1207 (934)	2031 (1758)	46.2	—	624
c-2	42.4	3.3	2.5	51.8	11	2.61	6.3	1218 (945)	2048 (1775)	47.8	—	629
c-3-S1	46.6	4.0	5.1	44.3	14	2.35	6.6	1210 (937)	1972 (1699)	39.8	—	501
c-3-S2	49.2	4.6	5.5	40.7	16	2.35	7.2	1209 (936)	1931 (1658)	36.0	—	436
c-3-S3	48.7	4.5	6.6	40.1	15	2.24	7.0	1204 (931)	1925 (1652)	35.3	—	431
c-3-S4	67.9	6.0	6.5	19.6	18	2.42	6.9	1212 (939)	1525 (1252)	13.1	—	13
c-4	42.3	3.4	3.5	50.8	12	2.49	6.3	1215 (942)	2038 (1765)	46.7	—	617
d-1	38.9	2.9	3.2	55.0	19	2.49	5.9	1215 (942)	2074 (1801)	51.2	—	697

in previous cells. It was studied by coring one sample of the cathode block (d-2). SEM-EDX analysis demonstrated that Sample d-2 was similar to deposit found at the center of the cell and may be an extension of it. In addition to the particular thick whitish deposits, the thin film in the intermediate zone tended to be generally more grayish and the CVD higher for Cell d than for Cell c. Table IV presents the summary of all sample chemical composition found in Zone 2 industrial cells.

Samples a-5, b-3, and c-5 were taken near the end of the ledge toe, while Sample d-2 seems to be the extension of the deposit of the central channel. The CR of the deposit of the cells a, b, and c showed very high CR (2.65 to 2.75), while Sample d-2 has a lower CR (2.43). The tendency to have less calcium in the thin film is again observed. Except for Sample d-2 that was thicker, all thin film samples had a similar or lower density than the metal pad.

D. Laboratory Experiments

The chemical composition and morphological properties of laboratory scale samples were obtained from six experiments using cells made of two different cathode materials (Table I). Each experiment had a side with a cooled wall to form a ledge toe and a smelting grade alumina (SGA) feeding side. The SGA feeding side was set to 1228 K (955 °C) and the temperature gradient between the two walls varied according to test parameters. Samples were collected three days after the cells were stopped allowing the cells to cool down through natural convection. The effects of the cathode material, heat transfer, and the feeding rate on the formation of the deposit were explored. Small scale of the laboratory cell and addition of alumina during the operation covered the very yellowish thin film normally found in industrial cells and generated mostly the grayish film in all of the six experiments. Table V summarizes the temperature gradient that existed between the wall near the SGA feeding and the cooled wall.

1. Effect of the cathode material
The tests A and B were performed using graphitized and 100 pct graphitic cathode material with their cooled wall under high heat transfer rate to maximize the ledge toe formation. An insulation setup, described in the

methodology section, helped increase the thermal gradient between the two sides. The concentration and property data for all samples are summarized in Table VI.

For both cells, a thin film was formed under the SGA feeding point (Figure 9) although it was much thinner for Test B. The deposits outside of the ledge toe (A-2, A-3, A-4, B-4, B-5) had an Al_2O_3 mass fraction between 17.1 and 23.8 pct and a CR between 2.23 and 2.41 which is similar to what can be found in Zone 1 Technology I deposit. Ledge toe on the cooled side of Test A was present and showed some characteristics found in the industrial cells (high concentration of cryolite, high CR, very low alumina concentration) but ledge toe from Test B was significantly longer and present another interesting characteristic. Postmortem analysis of Test B showed that the ledge toe did not form a smooth surface but was mixed with aluminum. The ledge toe samples (A-1, B-1, B-2, B-3) had an Al_2O_3 mass fraction of 10.1 pct for Test A and between 3.4 pct and 7.5 pct for Test B. CR was significantly higher for Test A (2.85) and for Test B (2.73 to 2.80) than for the rest of the deposit of the cell (2.23 to 2.41). The $CaF_{2(eq)}$ was also lower where a noticeable ledge toe was observed.

A thermodynamic study of the sample compositions enabled calculation of the temperature of crystallization of mainly Na_3AlF_6 and Al_2O_3. Calculations showed that other species ($Na_5Al_3F_{14}$, $Na_2Ca_3Al_2F_{14}$, $NaCaAlF_6$, and CaF_2) tend to crystallize along with Na_3AlF_6 generally with a mass fraction of about 10 pct at operation temperature but they were neglected. When the local temperature is lower than the temperature of crystallization of Na_3AlF_6 or Al_2O_3, these species will be present as solid during operation. The presence of a heap in the center of the metal pad suggests that this was the case in the present experiments.

Temperature of the bath was measured with a thermocouple inserted into the laboratory cell. The thermocouple was rapidly degraded by the bath but gave an approximate temperature value of 1223 K (950 °C). For both cells, a gradient in the Al_2O_3 mass concentration was observed from the SGA feeding side to the center of the cell under the metal pad. At 1223 K (950 °C), the sample found directly under the feeder had a lower Al_2O_3 solid mass fraction (10.3 pct (A-4) and 11.7 pct (B-5)) than toward the center (17.7 pct (A-2), 16.4 pct (A-3), and 18.0 pct (B-4)). For Test A, the Al_2O_3 concentration at 1223 K (950 °C) on the cooled side showed that the ledge toe was almost completely liquid but for Test B, and the solid Na_3AlF_6 mass fraction was at least 31.6 pct (B-2) and 17.4 pct (B-3). The temperature of the ledge being lower due to cooling of the wall, the Na_3AlF_6 solid mass fraction is even higher. Figure 9 presents the top view and front view of the electrolysis tests A and B.

The analysis of the cross-section of the cathode surface by SEM-EDX enabled the identification of the microstructures within the deposit and the position of the main elements. Typical microstructures of the thin film varied from the cooled wall side to the SGA feeding side (see Figure 10).

Near the cooled wall, the ledge toe deposit was between 1500- and 2500-μm thick. Hexagonal platelets made of aluminum and oxygen elements and associated to α-Al_2O_3 were observed at the cathode block interface and in the bulk of the deposit. The diameter of the detected particles ranged from 70 to 165 μm and had a thickness from 6 to 12 μm. A thin layer rich in aluminum was present at the very top of the cathode block interface and had a thickness of 70 to 130 μm. The layer was analyzed by SEM-EDX with a point & ID method and the carbon mass concentration reached up to 29.6 pct. While precise quantification was not possible with this technique, the presence of the carbon element could be ascertained and the thin layer was associated with Al_4C_3. Directly over the Al_4C_3 thin layer, an oxygen-rich thin layer was found and had a thickness between 20 to 60 μm.

Closer to the SGA feeding side of the cell, the thin film was between 110- and 400-μm thick. Hexagonal platelets made of α-Al_2O_3 were observed at the cathode block interface, in the bulk, and at the aluminum interface of the film. The particles detected had a diameter of 15 to 125 μm and a thickness of 3 to 4 μm. The thin Al_4C_3 layer had a thickness from 10 to 35 μm at the cathode surface. An oxygen-rich layer was sometimes present and had a thickness of 0 to 10 μm. Figure 10 shows a typical microstructure of a thin deposit from Test B.

2. Effect of the heat transfer

Test C was performed by using graphitized material and by reducing the heat transfer of the cooled wall to observe the effect of the heat transfer variation on the deposit formation. The deposit under the feeder was significantly thicker than Test A and Test B deposits at the same position. This counterintuitive result is discussed later in the paper. The ratio between the cathode block surface and the metal pad height in the industrial cells enables the metal pad to clearly separate the bath from the deposits. This is not the case in laboratory cells as vertical and horizontal dimensions are very similar. The sludge has to sink through the metal pad in industrial cells while it can get around the metal pad in laboratory cell.

Compared to Test A, solid Al_2O_3 mass fraction of the deposits under the SGA feeder increased from 10.3 pct (A-4) to 17.8 pct (C-4) giving a density at 1223 K (950 °C) greater than the metal pad. The same Al_2O_3 mass concentration gradient from under the feeder toward the center of the cell was still observed. The higher CR within Test C deposit was still observed near the cooled wall (2.40). However, the concentration gradient between the ledge toe and the deposit under the feeder was less significant than for Test A. Overall, $CaF_{2(eq)}$ concentration was higher for the low heat transfer experiment. Figure 11 presents the top view and front view of the electrolysis Test C.

3. Effect of an alumina plate at the cooled wall

Test D repeated the condition of Test C with the addition of an alumina plate on the cooled wall in order to identify its effect when a known surface area is needed
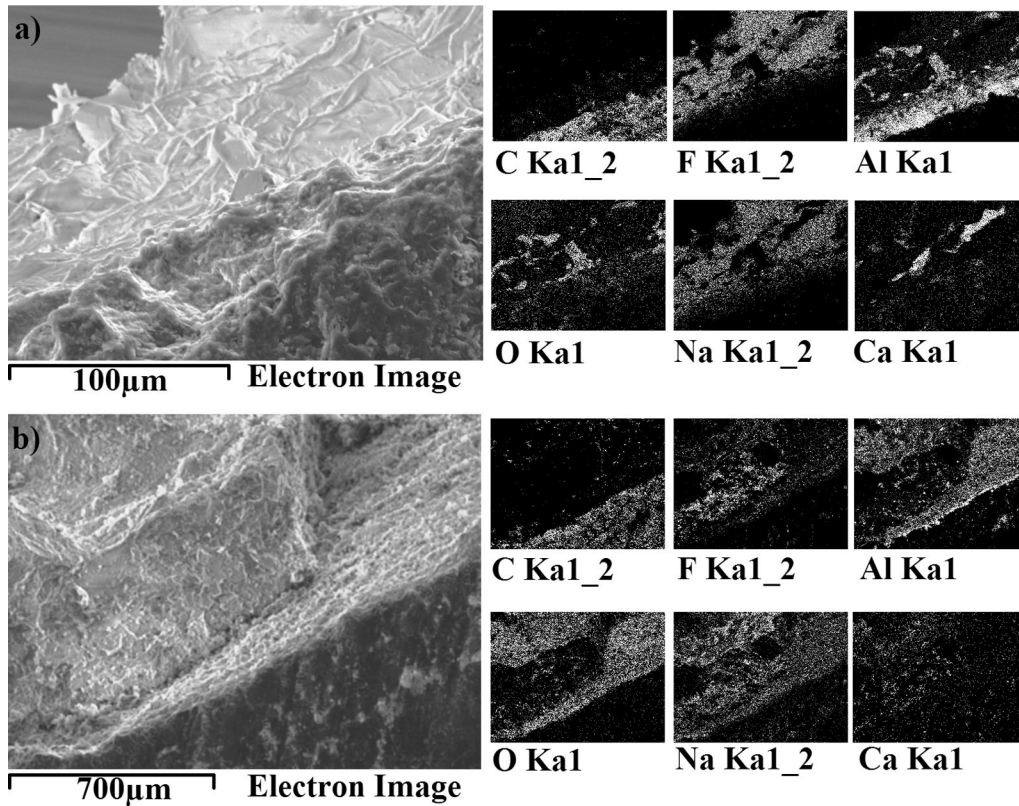
Fig. 8—MEB-EDX analysis of the (*a*) yellowish and (*b*) grayish thin film in the intermediate zone.

Table IV. Chemical Composition of Deposit in Zone 2 (Intermediate Zone)

Sample	Na_3AlF_6 (Pct)	CaF_2 (Pct)	AlF_3 (Pct)	Al_2O_3 (Pct)	Amorph. (Pct)	CR	$CaF_{2(eq)}$ (Pct)	$T_{crist.}$ Na_3AlF_6 K (°C)	$T_{crist.}$ Al_2O_3 K (°C)	$Al_2O_{3(s)}$ 1233 K (960 °C) (Pct)	$Na_3AlF_{6(s)}$ 1233 K (960 °C) (Pct)	$\Delta\rho$ 1233 K (960 °C) kg/m³
a-5	82.8	4.5	4.2	8.6	36	2.67	4.5	1222 (949)	1242 (969)	0.5	—	(261)
b-3	72.9	3.5	2.7	21.1	23	2.75	4.0	1224 (951)	1509 (1236)	13.9	—	(21)
c-5	78.8	5.5	4.2	11.5	14	2.65	5.7	1219 (946)	1310 (1037)	3.9	—	(185)
d-2	44.7	5.3	4.2	45.9	19	2.43	9.1	1208 (935)	1990 (1717)	41.8	—	544

Table V. Temperature Gradient between the Two Walls Depending on the Electrolysis Parameters

Test	Cathode Material	Heat Transfer Rate	Alumina Plate at the Cooled Wall	Average Temperature Gradient Between the Two Walls in K (°C)
A	Graphitized	High	No	32.4 ± 0.7
B	100 pct Graphitic	High	No	37.6 ± 1.9
C	Graphitized	Low	No	19.1 ± 1.0
D	Graphitized	Low	Yes	27.1 ± 1.1
E	100 pct Graphitic	High	Yes	43.3 ± 2.5
F	Graphitized	Low	No	16.0 ± 2.6

(*i.e.*, to evaluate the cathode current density). The average temperature gradient between the two carbon walls for Test D was 27.1 K ± 1.1 K (27.1 °C ± 1.1 °C) which was higher than Test C but did not mean that the temperature of the cooled wall on the operation side was lower because the alumina plate could act as a thermal isolator. One striking difference was the composition of sample D-1. Compared to Test C (C-1), the sample near
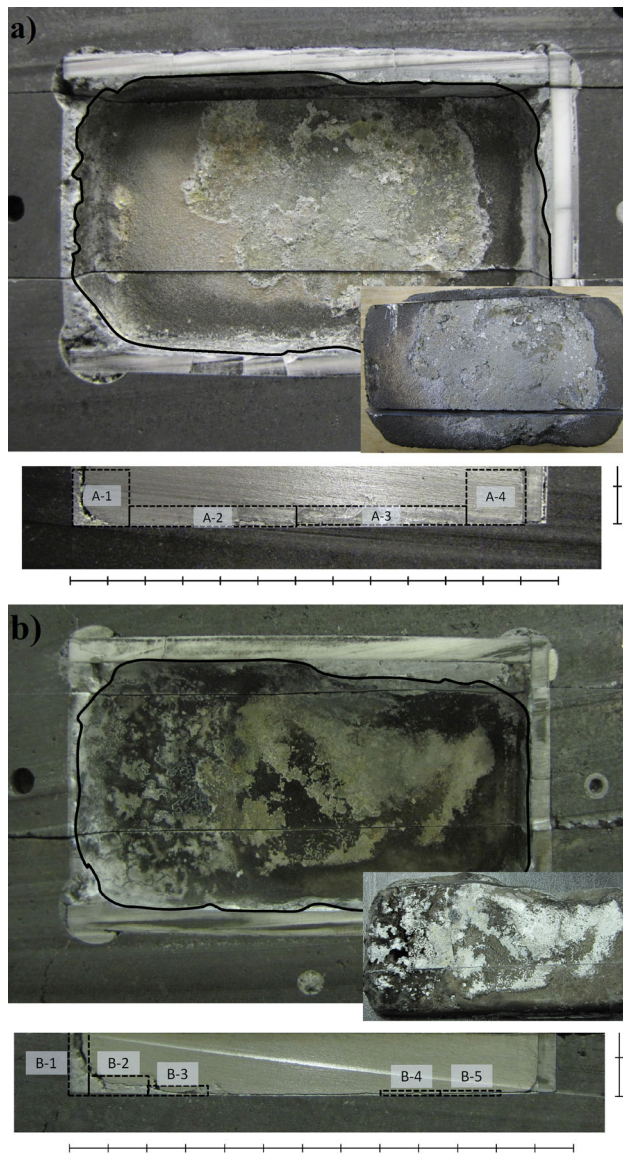
Fig. 9—Top view and front view of the deposit in (*a*) Test A and (*b*) Test B.

the cooled side (D-1) had a very high Al_2O_3 mass concentration (31.5 pct), and thus, no ledge toe was observed. The higher CR (2.87) was observed under the SGA fed side rather than near the cooled side (2.56). Under the metal pad in the middle of the cell, the thick deposit formed a heap in both tests C and D.

While the tests C and D produced a thick deposit, Test B produced a thinner one. To further our knowledge of the insulating effect from an alumina plate resulting in a thin film, Test E was performed with similar conditions to Test B by adding an alumina plate on the cooled side. The effect of cooling was evident when comparing to the tests C and D. In Test E, a noticeable ledge toe was produced in the corner of the cell while almost none could be observed in the tests C and D. The presence of solid Na_3AlF_6 at 1223 K (950 °C) in the thermodynamic model demonstrated the formation of ledge toe during operation. A thin film was

also present all over the base of the cell. Deposits under the SGA feeding point had an Al_2O_3 solid mass fraction (16.7 pct) higher than the deposits found near the cooled wall (13.8 pct) but the two deposits had a similar CR (2.77 for E-3 *vs* 2.75 for E-2). This is unusual as the deposit under the SGA feeding point is not near the high current density zone, close to the cooled wall, meaning that important transport existed between the two sides during operation. Figure 12 presents the top view and front view of the electrolysis tests D and E.

4. Overfeeding experiment

Test F was performed under similar conditions than Test C, but with 150 pct of the theoretical SGA feeding rate instead of 120 pct. Test F had a slightly lower temperature gradient between the 2 walls—16.0 K ± 2.6 K (16.0 °C ± 2.6 °C) than Test C but this was not significant, as the temperature difference was within the measurement standard deviation. While the amount of thick deposit coverage increased significantly, the Al_2O_3 mass concentration was not as high as expected for the samples of Test F compared to the sample of Test C. The CR values of the deposits in Test F were different from each other compared to Test C. Again, the deposit under the metal pad formed a heap similar to the tests C and D. Figure 13 presents the top view and front view of the electrolysis Test F.

SEM-EDX analysis was also used to identify the microstructures of the thick deposits. The total thickness of the deposits could reach several centimeters, but distinctive behaviors occurred when the deposit exceeded 700 μm. As shown in Figure 14, the behavior of the Al_4C_3 layer was similar for the deposits containing low (9.1 pct) and high (23.6 pct) mass concentrations of Al_2O_3. For thicknesses lower than 700 μm in the deposits, the Al_4C_3 layer was thinner and was mainly present within the cathode block. For deposits thicker than 700 μm, the Al_4C_3 layer was thicker and built up from the bottom of the deposit. Similar results were observed under a thick deposit in the middle of the cell in Test D. The Al_4C_3 layer went from an average of 30 to 70 μm when the thick deposit reached 700 μm. As for the α-Al_2O_3 hexagonal platelets, it was difficult to observe them in the thick deposits but their presence was confirmed by their isolation through washing of the cryolitic species with hot water. Figure 14 shows the typical microstructure a thick deposit from Test F. Table VI presents the summary of all sample chemical composition found in laboratory cells.

IV. DISCUSSION ON THE DEPOSIT FORMATION

A. *Deposit in Zone 1 at the Center of the Industrial Cells*

Incomplete alumina dissolution in industrial cell operation has been confirmed by a previous study.[6] Bath along with alumina may also sink through the metal-bath interface under specific agglomeration and density conditions.[7] While it is known that dispersion of the SGA fed along the central channel occurs,[9] the localized deposits in the cells a and b align more closely
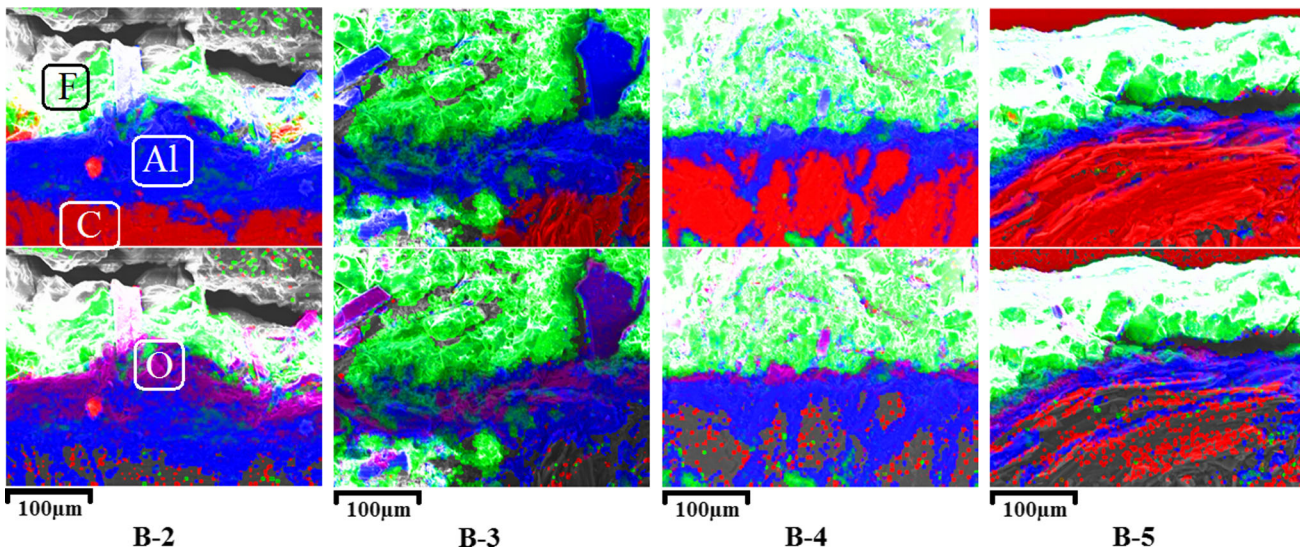
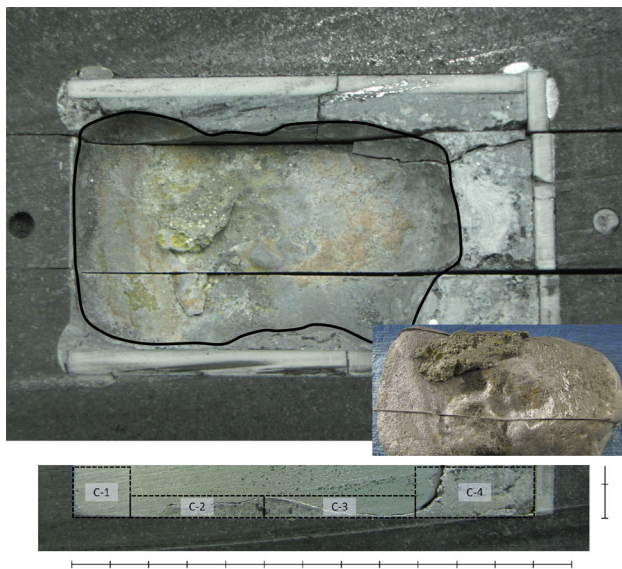Fig. 10—Typical microstructure of the ledge toe (*B-2* and *B-3*) and the thin film (*B-4* and *B-5*).

Fig. 11—Top view and front view of the deposit in Test C.

with the SGA feeders than the low velocity zones. Figure 5 illustrates that this phenomenon was not predominant in Technology I for the two postmortem cells.

Falling of the anode cover material, a mixture of crust bath and alumina protecting the anode, can cause disturbances in the alumina mass and energy balance of the cell.[16] It constitutes a difficult phenomenon both to predict and to quantify, but it most likely influences the presence of deposits along the central channel. As shown by Table II, the chemical compositions of the deposits in technologies I and II are significantly different in terms of total alumina content which suggests different formation types. The deposits at the center of the cells *a* and *b* contained an Al_2O_3 mass content higher than 9.3 pct but not higher than 33.3 pct. The position of the

deposits demonstrates incomplete dissolution where fine alumina particles sink through the metal pad along with frozen bath and accumulate just under the SGA feeders. Electrolysis at laboratory scale showed samples that contained a maximum of 29.2 pct for a highly overfed alumina experiment (150 pct of the theoretical value). It is therefore possible that incomplete dissolution produces a maximum alumina concentration threshold in the sludge that could explain why the deposits in the cells a and b have a lower Al_2O_3 mass concentration than deposits in the cells c and d. The deposits from the cells c and d contained an alumina mass content between 40.1 and 55.0 pct, if overlooking the peculiar Sample c3-S4 discussed later on. These concentrations are higher than the concentration found in the laboratory overfeeding experiment. Samples of the anode cover material in the central channel contained an alumina mass concentration from 37.5 to 59.0 pct.[17] The position of the deposits suggests block of anode covering material falling in the central channel.

When agglomerates sink through the metal pad, they mainly form deposits at the center of the cathode block. The frozen bath around the agglomerate melts and forms a layer at the top of the sludge if the alumina mass concentration is lower than 35 pct, but no free melt is observed if the alumina mass concentration is higher than 40 pct.[18] Results found in this study add to this behavior. The vertical alumina mass concentration gradient in Sample c-3 supports the formation of a suspension on the top of the deposits that remains below the metal pad. The Sample c-3-S4 top layer composed of low Al_2O_3 supersaturated bath has a local density close to the density of liquid aluminum. As shown in Table VII, the difference in density between the top layer and the liquid aluminum is positive or negative depending on the operating temperature.

This suspension formed on top of the dense deposit is thus free sludge and can be easily carried all over the cell by MHD-induced movement of the metal pad and can potentially cause backfeeding.[9]
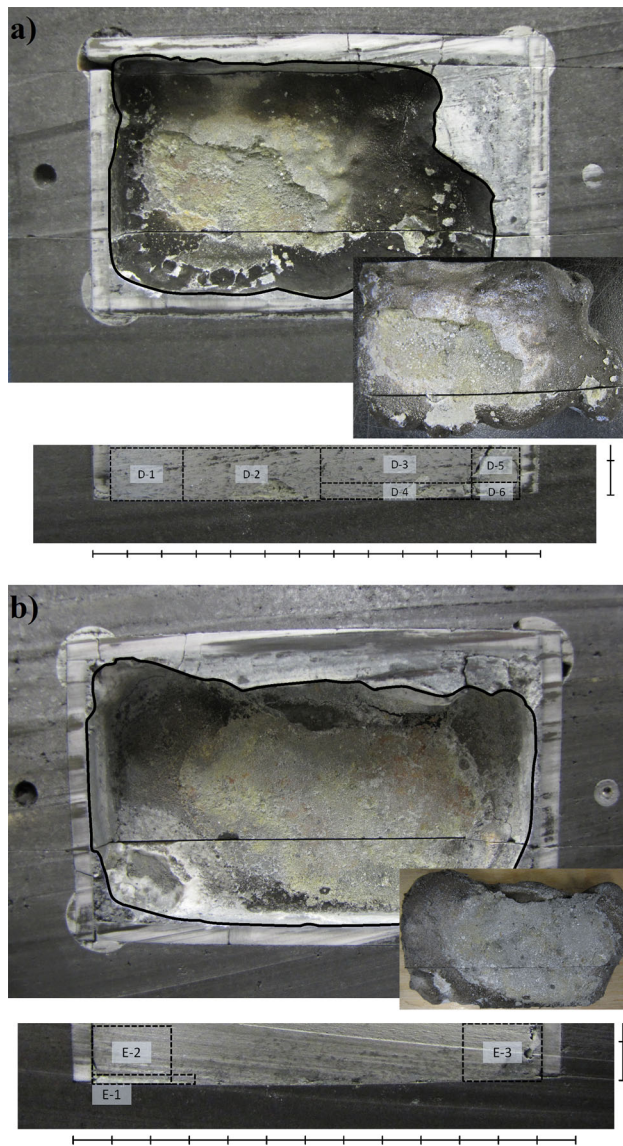
Fig. 12—Top view and front view of the deposit in (a) Test D and (b) Test E.

During the postmortem analysis of the cells c and d, almost no deposits along the central channel were observed on the cathode blocks. However, a dark stripe on the cathodes and deposits on the cooled metal pad suggested the presence of a thick deposit during operation removed during the preparation of the cell postmortem analysis. The same phenomenon occurred in the laboratory experiment where part of the deposit attached preferentially to the metal pad rather than to the cathode block. An Al_4C_3 layer of 400 to 700 μm was found under the thick deposit and showed that a chemical reaction occurred instead of an electrochemical reaction at this location of the cell. The SEM-EDX analysis from Test F (see Figure 14) showed that this Al_4C_3 layer is formed through diffusion at the bottom of the deposit. The later deposit along with the Al_4C_3 layer somehow protects the carbon cathode block. Under the

thin film, the Al_4C_3 layer is also thinner and forms preferentially in the binder of the cathode block causing the deterioration of the cathode block with a probable electrochemical reaction mechanism.[19,20] Significant variation of the CR in the deposit at the center of the cell and MHD-induced movements of the metal pad suggests exchange of material from the end of the ledge toe to the center and back.

B. Deposit in Zone 2 (Industrial Cells Intermediate Zone)

While no thick deposition is generally observed directly under the anodes, material can be brought in the intermediate zone by the movement of the deposits from the central channel and the ledge toe. In following studies, a particular attention should be given to the suspension on the top of the thick deposits. The visual aspect of the intermediate zone can vary from yellowish to grayish. Although the film was very thin (<1 μm) in the most yellowish zone, it was not possible to observe an area of the cathode surface where bath film was not present. This observation supports again the exchange of material between the end of the ledge toe and the central channel.

SEM-EDX analysis showed that the grayish film thickness could range from 0.5 mm to 1.5 mm. The sample contained an alumina mass fraction equal or inferior to a mass concentration of 20 pct. Thus, its corresponding density was inferior to the theoretical density required to remain below the metal pad. However, in the presence of liquid cryolite, aluminum in the presence of current is known to wet the carbon allowing an alumina supersaturated bath film to adhere to the surface of the cathode block. The grayish supersaturated bath film had a typically high CR (2.69) compared to the electrolysis bath (CR = 2.20).

Observed Al_2O_3 hexagonal platelets in the thin film can derive from the simple cooling of the cell, but evidence suggests that they were present during operation, for example, the supersaturation of the thin films. The deposition of pre-existing particles formed elsewhere in the cell remains probable, but local heat transfer conditions most likely influenced particle morphology and growth. These particles have been observed consistently in the samples taken in the intermediate zone in industrial cells. In laboratory tests, particles between 100 and 500 μm were also observed. The particle size was higher near the cooled wall and near interfaces.

Covered with a very thin bath film, the Al_4C_3 layer thickness varied between <1 to 15 μm and was found with a yellowish aspect. However, this work demonstrated that the presence of a supersaturated bath film of 0.5 to 1.5 mm was sufficient to homogenize the Al_4C_3 layer from 10 to 20 μm and potentially increase the resistivity locally. In both Technologies, thicker deposits in the intermediate zone where the highest current density is expected resulted in more grayish aspect and were correlated with higher CVD.

C. Effect of the Experimental Parameters on the Deposit Formation

A number of six experiments evaluated the effect of the cathode material, the heat transfer, the addition of an alumina plate, and overfeeding on the deposit formation.

1. Cathode material

The effect of the cathode material on deposit formation was mostly caused by the thermal conductivity of the two cathode materials. While graphitized cathode block from Test A is more conductive than 100 pct graphitic cathode

Fig. 13—Top view and front view of the deposit in Test F.

block from Test B, postmortem analysis showed that Test A produced less ledge toe than Test B. The mass concentration of the low solid alumina and even high solid cryolite demonstrated that heat transfer were more important for Test B than Test A supporting that higher heat transfer occurs for the 100 pct graphitic cathode block. This higher heat transfer rate in Test B was further supported by the greater temperature gradient between the two walls in Test B than in Test A. This counter intuitive result is explained by the fact that cooled wall from Test A thermally more conductive cathode block was more influenced by the external heat furnace than the cooled wall from Test B thermally less conductive cathode block. These results are limited to the effect of the cathode block and cannot be generalized to the different technologies.

2. Heat transfer rate

Several parameters in industrial cells may impact the heat transfer at the cathode block interface (anode change, anode effects, cell temperature, cell design, metal pad height, cell amperage, and formation of bottom deposits). Because heat transfer is hard to control in industrial cell, it becomes very interesting to control it in laboratory cells. It is important to note that laboratory heat transfer results are limited by the fact that industrial cell is autothermic and heat themselves just with the bath resistivity, which is not the case for the laboratory cells that have to be heated by an external source. Changing the heat transfer rate in laboratory cells intensified differentiation in deposit accumulation between Test A and Test C.

Low CR in the material of the ledge toe as well as lower temperature gradient between the two walls of Test C—19.1 K ± 1.0 K (19.1 °C ± 1.0 °C) compared
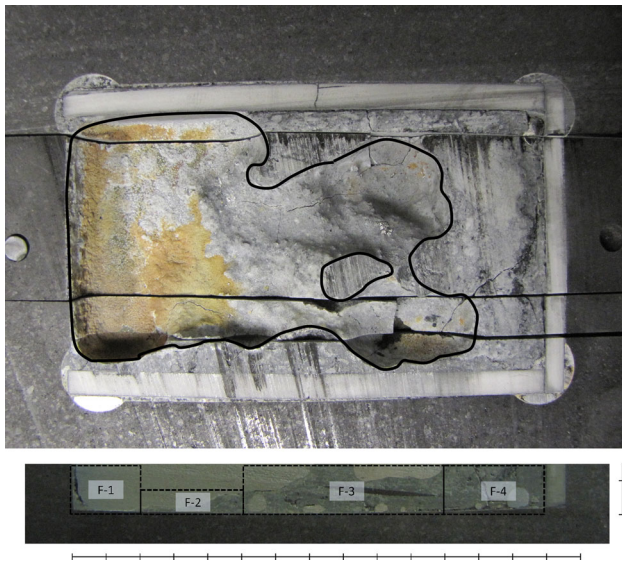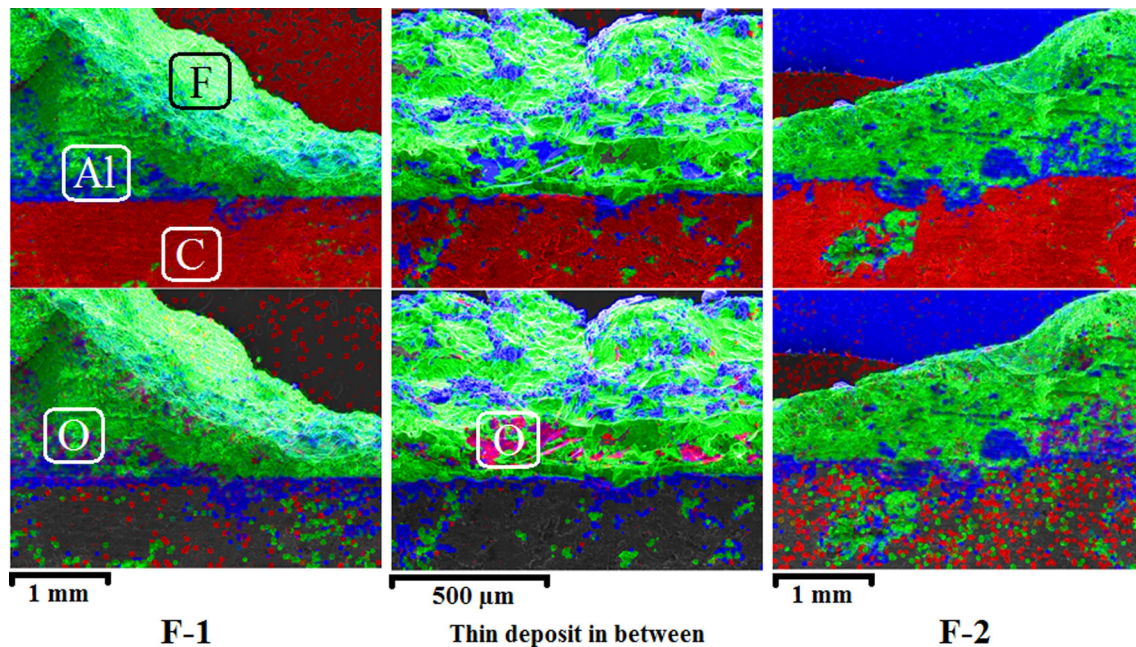

Fig. 14—Typical microstructure of the thick deposit (Test F).

Table VI. Summary of the Chemical Composition of the Deposit Found in the Laboratory Experiments

Sample	Na$_3$AlF$_6$ (Pct)	CaF$_2$ (Pct)	AlF$_3$ (Pct)	Al$_2$O$_3$ (Pct)	Amorph. (Pct)	CR	CaF$_{2(eq)}$ (Pct)	$T_{crist.}$ Na$_3$AlF$_6$ K (°C)	$T_{crist.}$ Al$_2$O$_3$ K (°C)	Al$_2$O$_{3(s)}$ 1223 K (950 °C) (Pct)	Na$_3$AlF$_{6(s)}$ 1223 K (950 °C) (Pct)	$\Delta\rho$ 1223 K (950 °C) kg/m^3
A-1	81.8	6.4	1.7	10.1	18	2.85	7.1	1220 (947)	1283 (1010)	3.1	—	(211)
A-2	63.6	5.3	7.5	23.7	26	2.32	6.9	1209 (936)	1631 (1 358)	17.7	—	107
A-3	65.7	4.5	7.2	22.6	30	2.36	5.9	1212 (939)	1592 (1 319)	16.4	—	74
A-4	71.7	4.2	7.0	17.1	20	2.41	5.1	1215 (942)	1441 (1 168)	10.3	—	(48)
B-1	86.1	3.9	2.5	7.5	10	2.80	4.3	1227 (954)	1224 (951)	1.9	—	(124)
B-2	88.6	4.4	3.5	3.4	36	2.73	4.6	1248 (975)	1219 (946)	—	31.6	(41)
B-3	87.6	4.5	3.3	4.5	34	2.74	4.7	1241 (968)	1216 (943)	—	17.4	(104)
B-4	63.7	5.5	7.0	23.8	27	2.35	7.2	1210 (937)	1633 (1360)	18.0	—	111
B-5	67.1	5.6	9.3	18.0	25	2.23	6.8	1205 (932)	1495 (1222)	11.7	—	9
C-1	75.4	8.4	7.6	8.7	22	2.40	9.2	1208 (935)	1271 (998)	2.1	—	(164)
C-2	60.1	6.0	7.8	26.0	6	2.26	8.2	1205 (932)	1696 (1423)	20.6	—	172
C-3	59.2	6.6	8.3	24.6	—	2.22	8.9	1202 (929)	1681 (1408)	19.3	—	158
C-4	63.9	5.2	7.1	23.7	13	2.35	6.9	1210 (937)	1627 (1354)	17.8	—	106
D-1	59.2	5.3	4.0	31.5	5	2.56	7.7	1215 (942)	1784 (1511)	26.3	—	246
D-2	71.4	7.3	4.9	16.5	23	2.56	8.7	1217 (944)	1448 (1175)	10.2	—	(40)
D-3	67.6	4.2	3.5	24.7	22	2.65	5.6	1221 (948)	1617 (1344)	18.6	—	84
D-4	67.9	5.6	3.0	23.5	23	2.70	7.3	1218 (945)	1600 (1327)	17.6	—	73
D-5	74.0	4.1	3.8	18.1	12	2.66	5.0	1222 (949)	1449 (1176)	11.3	—	(55)
D-6	71.5	5.7	1.3	21.5	21	2.87	7.2	1219 (946)	1540 (1267)	15.4	—	17
E-1	87.8	6.4	1.9	3.9	—	2.84	6.6	1239 (966)	1216 (943)	—	12.9	(115)
E-2	70.8	6.8	2.6	19.8	—	2.75	8.5	1215 (942)	1516 (1243)	13.8	—	6
E-3	72.8	3.2	2.5	21.6	—	2.77	4.1	1225 (952)	1518 (1245)	16.7	—	134
F-1	80.4	5.4	5.1	9.1	21	2.59	5.9	1219 (946)	1258 (985)	1.6	—	(221)
F-2	67.2	5.1	4.1	23.6	5	2.61	6.7	1218 (945)	1604 (1 331)	17.6	—	77
F-3	61.5	5.0	4.4	29.2	14	2.55	7.0	1216 (943)	1736 (1 463)	23.7	—	196
F-4	0.6	5.0	4.1	28.8	7	2.57	7.0	1216 (943)	1726 (1 453)	23.3	—	186

Table VII. Comparison of the Liquid Aluminum and the Sample c-3 and c3-S4 in Function of the Temperature

Temperature in K (°C)	1213 (940)	1223 (950)	1233 (960)	1243 (970)	1253 (980)
Metal density (kg/m^3)	2303.8	2302.0	2300.1	2298.3	2296.5
Estimated density of c3	2488.3	2484.4	2480.5	2476.6	2472.7
Difference	184.5	182.5	180.4	178.3	176.3
Estimated density of c-3-S4	2305.5	2301.0	2296.5	2292.0	2287.5
Difference	1.7	−1.0	−3.6	−6.3	−8.9

to Test A—32.4 K ± 0.7 K (32.4 °C ± 0.7 °C) and Test B—37.6 K ± 1.9 K (37.6 °C ± 1.9 °C) all confirmed lower heat transfer rate for Test C. More bottom sludge accumulated when lower heat transfer was imposed. This other counter intuitive result needs that a distinction be made between cold cells and hot cells under high heat transfer. Cells from tests A, B, and C were of similar temperature near the SGA feeder and would normally generate the same amount of bottom sludge. Higher heat transfer in tests A and B cooled wall enabled more cryolite to precipitate than in Test C, and thus, more ledge toe was form in tests A and B. MHD-induced movement transported ledge toe deposit toward the center of the cell and resulted in the reaction with bottom sludge and subsequent generation of liquid deposit lesser dense than aluminum. Ledge toe formation was sufficient to consume the bottom deposit under the feeder for tests A and B but not for Test C. This movement of the ledge toe toward the center of the cell could well explain why CR value can be as high as 2.63 in industrial cell Zone 1 deposits.

3. Addition of an alumina plate

Insulating the cooled wall and therefore reducing the ledge toe formation was the main effect of adding a fourth alumina plate. Electrolysis experiment in laboratory with and without alumina plate in regard to the measured temperature gradient between the cooled side and the SGA feeder side had to be treated differently. The alumina plate in itself brought an additional heat barrier that prevented cooling of the wall while decreasing the temperature measured by the thermocouple. The measured temperature gradient on the cooled side became relevant when comparing Test D—27.1 K ± 1.1 K (27.1 °C ± 1.1 °C)—and Test E—43.3 K ± 2.5 K (43.3 °C ± 2.5 °C)—that both contain a fourth alumina plate.

Parameters in Test C allowed for low heat transfer and a larger amount of sludge to be produced. The addition of an alumina plate in Test D lowered the heat transfer even more. The low CR (2.56) and high alumina mass concentration (31.5 pct) in Sample D-1 confirmed that more sludge was produced and then probably

brought to the other side of the cell through MHD-induced movements of the aluminum pad.

Parameters in Test B allowed for high heat transfer and ledge toe formation causing low SGA bottom sludge to be produced. In the case of Test E, the addition of an alumina plate decreased the heat transfer and hindered ledge toe formation. High heat transfer imposed on the cooled wall was found to be sufficient to form the ledge toe through the corner in Test E, but the greater amount of undissolved SGA and higher alumina mass concentration in Sample E-3 than in Sample B-5 confirmed that ledge toe formation was hindered.

4. Overfeeding

SGA overfeeding forced undissolved alumina to accumulate in Test F bottom floor and filled the cell quickly (3.5 h) until the voltage rose and caused the experiment to stop prematurely. Test F maximum alumina mass concentration (29.2 pct) was similar for samples a-1 (33.0 pct) and a-3 (33.3 pct) in Zone 1 Technology I deposit, while it was significantly lower than sample c-1 (50.2 pct), c-2 (51.8 pct), c-4 (50.8 pct), and d-1 (55.0 pct) in Zone 1 Technology II deposits. These results showed that deposits in Zone 1 Technology II could not be formed only by SGA incomplete dissolution.

D. Comparison Between Laboratory and Industrial Cells

The composition analysis of all laboratory samples enabled a clear distinction between ledge toe and bottom sludge deposits. Bottom sludge deposits in terms of alumina concentration, CR, and CaF_{2eq} possessed characteristic composition of the Zone 1 deposit in Technology I for all experiments that did not have an alumina plate on the cooled wall. Some samples under the feeder in Test D and Test E had an unusually high CR that might have been caused by a significant change in the MHD pattern but this would need further investigation.

Thick deposits in laboratory cells were undissolved SGA that sank at the bottom of the cathode block. This was especially verified for Test F deposits that were produced through SGA overfeeding. The ledge toe was formed through cryolite precipitation caused by the cooling of the wall. This was also supported by all laboratory experiments that did not contain a fourth alumina plate. Ledge toe formation was nevertheless verified in the corner of Test E cell even if it contained a fourth alumina plate.

The formation of an aluminum density like deposits as found in industrial sample c-3-S4 was supported by some bottom sludge deposits. Estimated differential densities between liquid aluminum and samples A-4 (-48 kg/m^3), B-5 (9 kg/m^3) D-2 (-40 kg/m^3), and D-5 (-55 kg/m^3) were close to zero. No sample was found to contain estimated solid mass concentration between 3.1 and 10.2 pct. This is an expected result as deposit with lower solid alumina mass concentration would have an insufficient density to remain under the aluminum pad. Ledge toe deposits in laboratory cells had very low estimated density at 1223 K (950 °C) but they were

certainly cooler than that. Thermodynamic study pointed that cooler ledge toe deposits contained even more solid cryolite than estimated and were thus denser.

MHD occurred in laboratory setup but in a much lower intensity than in industrial cells due to different metal pad height/length ratio and cell dimensions. The MHD-induced movement of the aluminum pad although smaller than in the industrial cells caused ledge toe and bottom sludge deposits displacement. This displacement of the two types of deposit resulted in the formation of a heap in the center of laboratory cells, the formation of a grayish film typically found in industrial cell intermediate zone, and the generation of a completely liquid deposit that backfeed in the bath due to its lower density. It is important to note that while higher heat transfer tended to form more ledge toe and seemed to eliminate the bottom sludge in laboratory cells, high heat transfer in industrial cells would probably enhance both the ledge toe and the thin resistive film in the intermediate zone as they looked to grow together.

In industrial cells, Al_4C_3 sublayer thickness was found to increase as the grayish film thickness increased. This phenomenon was supported in laboratory experiments through SEM-EDX analysis. It was observed in Test B that the Al_4C_3 layer near the SGA feeding side had a thickness from 10 to 35 μm when the thin film was between 110- and 400-μm thick and between 70 and 130 μm on the cooled side under the 1500- to 2500-μm thick ledge toe.

SEM-EDX analysis demonstrated also that the Al_4C_3 layer accumulated within the deposit (Figure 14) and supported a mass transport-driven formation when the deposit thickness exceeded 700 μm in laboratory experiments. This phenomenon was observed in Test D near Sample D-2 in the center of the cell where the Al_4C_3 layer went from an average of 30 to 70 μm when the thick deposit reached 700 μm. In Test F, this phenomenon was observed both for ledge toe and for bottom sludge deposits.

The oxygen-rich layer along with the Al_4C_3 layer identified in Test B and Test F supported the formation of oxycarbide previously discovered through XPS analysis.[20] While this phenomenon was hardly observed in the industrial cell deposit samples, laboratory cell experiments were found useful to identify this phenomenon.

V. SUMMARY AND CONCLUSIONS

The postmortem analysis of bottom deposits in four industrial aluminum electrolysis cells from two technologies enabled to make the distinction between three zones being the center, the ledge toe, and an intermediate zone. Deposition in the center of the cells showed two types of deposition depending on the technology:

– A thin deposit a few millimeters thick just below the SGA point feeders for Technology I cells;
– A deposit a few centimeters thick along the central channel which was easy to remove. A dark stripe was found under this deposit on the cathode block floor

during the postmortem analysis of Technology II cells.

These deposits are not linked with the ledge toe extending toward the center of the cell. Thin deposits in the center of Technology I cells contained an Al_2O_3 mass concentration higher than 9.3 pct but not higher than 33.3 pct. Laboratory experiments support that they are formed by SGA incomplete dissolution as they are positioned directly under the SGA feeders and possess similar chemical composition than when laboratory samples were obtained through forced incomplete dissolution. Furthermore, the velocity profile does not present dead zones that would promote deposit accumulations in that area. The deposition phenomenon in the central channel of Technology II cells could not be established with certainty. However, anode cover material collapse is a known phenomenon that could explain the presence of sludge in the central channel.

Vertical composition analysis of a typical sample found in the central channel demonstrated the presence of an alumina supersaturated bath top layer in this deposit. This top layer had a similar density to liquid aluminum at operating temperatures and was also observed in laboratory experiments. This top layer contained a significantly higher liquid fraction than the rest of the deposits. This made it more susceptible to be displaced by the metal pad MHD-induced movement.

A thin film was found in the intermediate zone in between the ledge toe and the thick deposit in the central channel. The thin film chemical composition and liquid fraction imparted a density equal or inferior to liquid aluminum. Its presence further established the material exchange between the deposits in the central channel and the ledge toe. In both Technologies, thicker deposits in the intermediate zone where the highest current density is expected resulted in more grayish aspect and were correlated with higher CVD.

The thermal conductivity of the cathode block affected deposit formation in the laboratory experiments by increasing heat transfer. According to the literature, the conductivity ratio of the two types of blocks material may reach 2 or 3 at operating temperature. High heat transfer in general increased the formation of ledge toe that interacted with the bottom sludge that formed a liquid deposit. This liquid deposit less dense than aluminum backfed into the electrolytic bath. It is important to note that while this seemed beneficial, high heat transfer in industrial cells would probably enhance both the ledge toe and the thin resistive film in the intermediate zone as they looked to grow together in industrial cells.

It was concluded that a carbide layer systematically covered the cathode block. This could be demonstrated from the SEM-EDX and XRD analysis from both laboratory and industrial samples. This carbide layer was not uniform and contained electrolytic bath species. The carbide layer thickness could vary from tens to hundreds of microns depending on the sludge deposit thickness. The electron microscopy study revealed that the carbide layer could reach 10 to 20 μm in the intermediate zone when protected by a thin grayish film 0.5- to 1.5-mm thick.

In order to confirm the origin of the deposits formation along the central channel, an exhaustive study of anode cover material will need to be conducted. The effect of the adjacent thin film presence will be evaluated. Finally, further testing would permit the development of new procedures and cell designs reducing the deposit formation.

REFERENCES

1. P.Y. Geay, B.J. Welch and P. Homsi: *Light Met. 2001, Proc. Int. Symp.*, 2001, pp. 541–47.
2. L.N. Less: *Metall. Trans. B*, 1977, vol. 8B, pp. 219–25.
3. D. Whitfield, M. Skyllas-Kazacos, B. Welch and F.S. McFadden: *Light Met. 2004, Proc. Int. Symp.*, 2004, pp. 249–55.
4. F. Allard, G. Soucy, and L. Rivoaland: *Metall. Trans. B*, 2014, vol. 45B, pp. 2475–85.
5. M. Sørlie and H.A. Øye: *Cathodes in Aluminium Electrolysis*, 3rd ed., Aluminium-Verlag, Düsseldorf, 2010, p. 165.
6. V. Dassylva-Raymond, L.I. Kiss, S. Poncsak, P. Chartrand and J.F. Bilodeau: *Light Met. 2014, Proc. Int. Symp.*, 2014, pp. 603–608.
7. R. Keller: *Light Met. 2005, Proc. Int. Symp.*, 2005, pp. 147–50.
8. Y. Feng, M.A. Cooksey and M.P. Schwarz: *Light Met. 2011, Proc. Int. Symp.*, 2011, pp. 543–48.
9. K. Tørklep, K. Kalgraf and T. Nordbø: *Light Met. 1997, Proc. Int. Symp.*, 1997, pp. 377–86.
10. J. Thonstad, S. Rønning and P. Entner: *Light Met. 1982, Proc. Int. Symp.*, 1982, pp. 485–97.
11. D. Dumas and P. Lacroix: *Light Met. 1994, Proc. Int. Symp.*, 1994, pp. 751–60.
12. A. Solheim: *Alum. Trans.*, 2000, vol. 2, pp. 162–168.
13. R.G. Munro: *J. Am. Ceram. Soc.*, 1977, vol. 80, pp. 1919–28.
14. D. Dolejs and D.R. Baker: *Am. Miner.*, 2006, vol. 91, pp. 97–103.
15. F. Allard, M.A. Coulombe, G. Soucy and L. Rivoaland: *Light Met. 2014, Proc. Int. Symp.*, 2014, pp. 1233–38.
16. M. LeBreux, M. Desilets, A. Blais and M. Lacroix: *Light Met. 2014, Proc. Int. Symp.*, 2014, pp. 655–60.
17. F. Allard, M. Desilets, M. LeBreux and A. Blais: *Light Met. 2015, Proc. Int. Symp.*, 2015, pp. 565–70.
18. J. Thonstad, P. Johansen and E.W. Kristenson: *Light Met. 1980, Proc. Int. Symp.*, 1980, pp. 227–39.
19. P. Rafiei, F. Hiltmann, M. Hyland, B. James and B.J. Welch: *Light Met. 2001, Proc. Int. Symp.*, 2001, pp. 747–52.
20. M.A. Coulombe, M. Lebeuf, N. Fairley, J. Walton, and G. Soucy: *J. Electron Spectrosc. Relat. Phenom.*, 2012, vol. 185, pp. 588–97.
21. S. Renaudier, B. Bardet, G. Steiner, A. Pedcenko, J. Rappaz, S. Molokov and A. Masserey: *Light Met. 2013, Proc. Int. Symp.*, 2013, pp. 579–84.